Journal of Inorganic and Organometallic Polymers and Materials
https://doi.org/10.1007/s10904-023-02982-5

RESEARCH

Preparation of Two Transition Metal Coordination Polymers and Their Application as Photocatalysts in Dye Degradation

Jing Li[1] · Hongjiang Ren[1] · Jiangtao Li[1] · Liuchang Wang[1]

Received: 12 October 2023 / Accepted: 21 December 2023

Abstract
In the present study, two transition metal CPs on the basis of Co(II) and Mn(II) ions as the metal centers have been produced in success with reaction between the ligand of 2-(hydroxymethyl)-1*H*-benzo[*d*]imidazole-5-carboxylic acid (H_2L) and corresponding metal salts under a solvothermal reaction condition, and their chemical formulae are $\{[Co_2(HL)_2(H_2O)_4]\cdot H_2O\cdot SiF_6\}_n$ (**2**) together with $\{[Mn_2(HL)_2(H_2O)_3(SO_4)]\cdot H_2O\}_n$ (**1**). They were characterized by PXRD, EA, IR, single-crystal X-ray diffraction, and TGA. Additionally, both complexes exhibited excellent photocatalytic activity in the UV-induced degradation of Rhodamine B, rendering them excellent candidates for dye degradation.

Keywords Coordination polymer · Photocatalyst · Dye degradation · Rhodamine B(RhB)

1 Introduction

With the rapid development of industries, the pollution caused by industrial waste has become increasingly hard to ignore. Water pollution, in consideration of drinking water safety, has emerged as one of the pressing issues. Pollutants such as heavy metal ions from industrial wastewater, antibiotics overused in livestock farming, and dyes discharged untreated from textile and dyeing industries pose significant threats to water system safety [1–3]. Among these, organic dyes, due to their poor biodegradability and short-term chemical stability, constitute a major concern and require urgent treatment. Exploring an efficient, environmentally friendly, and cost-effective method to treat dye pollutants in wastewater is of paramount importance.

Metal-organic frameworks (MOFs), as a rapidly advancing class of materials, have garnered attention for their excellent stability, large surface area, and facile modifiability. They find applications in various fields including fluorescence, gas storage, drug loading, and catalysis [4–9]. According to some published literature, scientists have explored the use of metal-organic coordination polymers, including zinc and cadmium, as photocatalysts in the degradation of antibiotics and organic dyes [10–12]. Additionally, MOFs constructed with cobalt and manganese ions often exhibit excellent photocatalytic activity, offering potential for photocatalytic dye degradation to aid in wastewater treatment, thereby diversifying the range of photocatalytic materials.

It is well-known that the activity and structural diversity of MOFs largely depend on the choice of metal atoms and organic ligands, as well as the reaction mechanisms to obtain the coordination compounds [13, 14]. Therefore, the logical design of suitable metal ions and organic ligands plays a crucial role in synthesizing CPs with desirable properties. The benzimidazole moiety, being bicyclic and composed of imidazole and benzene rings, is widely used in the design and synthesis of photocatalysts [15–17]. To create MOFs with photocatalytic activity, aside from selecting appropriate active metal ions, the choice of suitable organic ligands is equally vital [18, 19]. Taking these factors into consideration, in this study, 2-(hydroxymethyl)-1*H*-benzo[*d*]imidazole-5-carboxylic acid (H_2L) was employed as the organic ligand to react with corresponding metal salts, resulting in the successful synthesis of two transition metal CPs with Cu(II) and Mn(II) ions as metal centers. Their structures were characterized through PXRD, EA, IR, single-crystal X-ray diffraction, and TGA analyses. Furthermore, the

✉ Liuchang Wang
wlg_112@163.com

[1] The Key Laboratory for Surface Engineering and Remanufacturing in Shaanxi Province, Key Laboratory of Chemistry of New Material of Functional Inorganic Composites, School of Chemical Engineering, Xi'an University, Xi'an, Shaanxi, China

Published online: 11 January 2024

photocatalytic degradation performance of the two materials towards the common dye Rhodamine B (RhB) under ultraviolet (UV) light irradiation was investigated [20–22]. The results revealed that both materials exhibited excellent photocatalytic performance for RhB degradation under UV light irradiation, with the degradation efficiency of 88.52% (**1**) and 80.16% (**2**) achieved after 150 min of UV irradiation. Furthermore, both materials maintained a relatively high degradation efficiency even after 5 cycles. Therefore, both materials have significant potential for the treatment of dye-containing wastewater.

2 Experimental

2.1 Chemicals and Measurements

In this work, all the chemical reagents for producing the complexes with reagent grade were purchased from market source and utilized with no further modifications. A PE 240 C automatic analyzer (Perkin-Elmer, Waltham, USA) was performed for conducting the EA of N, H and C at an analysis center of Liaoning Normal University. TGA were implemented with the PerkinElmer Diamond TG/DTA with 10 ℃ per min raising rate in a temperature range from RT to 800 ℃. With the Advance-D8 that containing a Cu-Kα radiation of $5° < 2\theta < 40°$, the PXRD could be performed at 2 s/step count time and 0.02° (2θ) step size. The IR spectra was gathered with Bruker AXS TENSOR-27 (Bruker, Karlsruhe, Germany) using pressed KBr pellets at RT from 400 to 4000 cm^{-1}. UV-visible absorption spectra were measured and recorded using a Shimadzu UV-2600 spectrophotometer. Data collection was conducted within the range of 200 to 400 nm. Dye degradation experiments were performed by placing 50 mg of the complex into a 1 L solution of 10 mg/L Rhodamine B (RhB) in water. After a certain period, 5 ml of the solution was extracted, and the degradation rate was studied using UV spectroscopy. The change in degradation rate over time was investigated.

2.2 Preparation and Characterization for $\{[Mn_2(HL)_2(H_2O)_3(SO_4)]\cdot H_2O\}_n$ (1) and $\{[Co_2(HL)_2(H_2O)_4]\cdot H_2O\cdot SiF_6\}_n$ (2)

A mixture synthesized from 0.1 mmol and 0.019 g of H_2L, 0.030 g and 0.2 mmol of $MnSO_4$, together with 5 mL of CH_3CN/H_2O (the volume ratio is 1:1) was stored in a stainless steel vessel (25 mL) lining by Teflon, and this mixture was heated under a temperature of 140 °C for twenty-four hours. After cooling this mixture RT with a cooling rate of 5 ℃ per h, the yellow crystals for the compound **1** were gathered with 42% of yield (in the light of H_2L). Anal. Calcd for $C_{18}H_{22}N_4O_{14}SMn_2$ (%): N, 8.48, C, 32.74 and H, 3.36. Found: N, 8.52, C, 32.50 and H, 3.68.

A mixture formed by 0.1 mmol and 0.019 g of H_2L, 0.031 g and 0.1 mmol of $CoSiF_6{\cdot}6H_2O$, together with 5 mL of $CH_3OH/CH_3CN/H_2O$ (the volume ratio is 3:1:1) was stored in a stainless steel vessel (25 mL) lining by Teflon, and this mixture was heated under a temperature of 130 °C for 72 h. After cooling this mixture RT with a cooling rate of 5 ℃ per h, the pink crystals for the compound **2** were gathered with 41% of yield (according to H_2**L**). Anal. Calcd for $C_{18}H_{24}N_4O_{11}F_6SiCo_2$ (%): N, 7.65, C, 29.52 and H, 3.30. Found: N, 7.53, C, 29.51 and H, 3.38.

The SuperNova was utilized for acquiring the data of X-ray. And the CrysAlisPro was employed for analyzing the intense data, and it was next converted to HKL files. The SHELXS in the light of direct mean together with the SHELXL-2014 software according to least-squares strategy were employed respectively for the synthesis and refinement of original architectural modes. After the use of entire non-hydrogen atoms, we mixed anisotropic parameters. Ultimately, the whole H-atoms were next fixed on the C atoms, which are bridged with AFIX commands in the geometry. The as-prepared compounds' refinements details as well as their crystallography parameters were displayed in the Table 1.

3 Results and Discussion

3.1 Crystal Structures

The analysis of single crystal X-ray diffraction displays that the **1** exists in a monoclinic *P*2(1)/*c* space group and it exhibits 2-dimensional coordination polymer net. There exist two isolated Mn(II) centers in crystallography, three coordinating molecules of H_2O, two H_2L, a SO_4^{2-} ion and a lattice molecule of H_2O in its structural unit. The Mn1 ion and Mn2 ion, two special cobalt ions, they possess a 6-coordinated geometry, where the Mn1 ion is coordinated via a N atom and a hydroxyl O atom come from two H_2O molecules and a HL^- unit, two carboxylic O atoms originated from two diverse H_2L (Fig. 1a). A N2 atom and O12, O6, O1 atoms occupied equatorial plane, while the four equatorial atoms are nearly coplanar with the Mn1 ion, and the average deviation is 0.080 Å. O2 atom and O13 atom are situated in axial locations; the center of Mn2 is surrounded through two carboxylic O donors existed in two diverse H_2L, a N atom and a hydroxyl O atom originated from a HL^- unit, a molecule of H_2O and a O atom in sulphate ion. N3 atom (N3) and O7, O4, O3 atoms occupied equatorial plane, but the four equatorial atoms are nearly coplanar with Mn2 ion, and the average deviation is 0.026 Å, O5 atom

Table 1 The CPs' refinements details as well as their crystallography parameters

Identification code	1	2
Empirical formula	$C_{18}H_{21}Mn_2N_4O_{14}S$	$C_{18}H_{24}Co_2F_6N_4O_{11}Si$
Formula weight	659.33	732.36
Temperature/K	296.15	273.15
Crystal system	monoclinic	triclinic
Space group	$P2_1/c$	P-1
a/Å	7.5160(10)	7.5127(2)
b/Å	11.038(4)	10.55980(10)
c/Å	27.714(2)	15.3692(3)
α/°	90	81.672(2)
β/°	95.163(3)	80.447(2)
γ/°	90	88.4920(10)
Volume/Å^3	2289.9(9)	1189.69(4)
Z	4	2
ρ_{calc}g/cm^3	1.912	2.044
μ/mm^{-1}	1.280	1.563
Data/restraints/parameters	3976/1/361	4179/17/415
Goodness-of-fit on F^2	1.080	1.102
Final R indexes [I >= 2σ (I)]	$R_1 = 0.0795$, $\omega R_2 = 0.2217$	$R_1 = 0.0241$, $\omega R_2 = 0.0594$
Final R indexes [all data]	$R_1 = 0.0891$, $\omega R_2 = 0.2282$	$R_1 = 0.0280$, $\omega R_2 = 0.0610$
Largest diff. peak/hole / e Å^{-3}	2.05/-0.79	0.23/-0.34

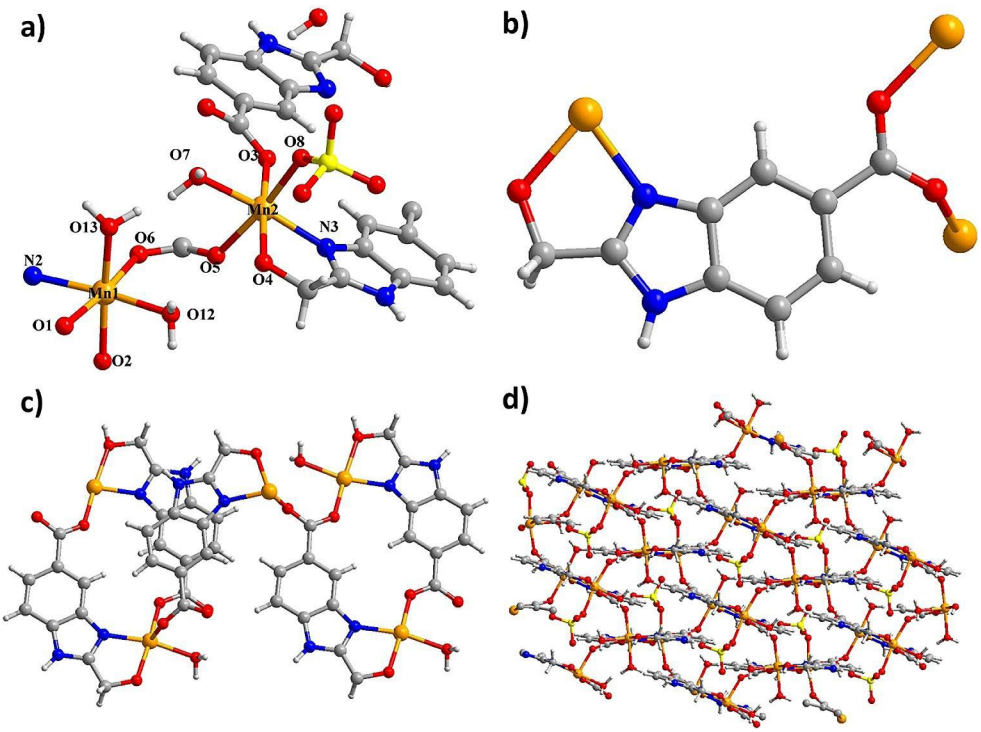

Fig. 1 (a) The diagram of the **1**'s least building unit. (b) The coordination manner of the ligand. (c) The 1-dimensional chain exits in compound **1**. (d) **1**'s 2D layered net

and O8 atom are situated in the axial locations. The Mn1 center and Mn2 center are situated in the twisted octahedral coordination structure of [$MnNO_5$]. In the complex **1**, the tetradentate ligand of H_2L is linked with two Mn(II) by the bidentate chelating carboxylic acid group of H_2L, hydroxyl-O atom and imidazole-N atom of this ligand, exhibiting a (κ^1-κ^1)-(κ^1)-(κ^1)-μ_3 coordination pattern (Fig. 1b). Fascinatingly, the O6, O4, O3, O1, N3, and N2 atoms in H_2L anion connect two metal atoms in order to establish a cyclic dimer subunit of [Mn_2(H**L**)$_2$]. In meantime, two repeating units are interlinked *through* μ_2-1,3-carboxylic acid links to generate a chain architecture in Fig. 1c. Besides, the consecutive chains are bridged via μ_2-1,3-carboxylic acid, which deeply consolidate the architecture, resulting in a 2-dimensional layered architecture by *ab*-plane, and the square dimensions is 4.9635 × 11.1578 Å^2 (Fig. 1d).

As exhibited by the detection of single-crystal X-ray diffractions, the **2** exits in the triclinic *P*-1 space group as a

2-dimensional coordination polymer (Fig. 2a), and its structural unit is composed of four coordinating molecules of H_2O, two coordinating H_2L, the isolated Co1 and Co2 ions in crystallography, a lattice H_2O molecule and a guest SiF_6^{2-} ion. The Co1 center and Co2 center reveal a coordination environment of [$CoNO_5$], with twisted octahedral structures. In the **2**'s crystal architecture, Co1 ion and Co2 ion are situated in completely distinct coordination surroundings. Co1 atom and Co2 atom are surrounded by two carboxylic acid O atoms, a hydroxyl O atom and a N atom provided by a HL^- unit, and two H_2O molecules, O8, O3 and O2 atoms and N1 atom occupied equatorial plane. As for the Co1 atom, the average deviation from plane is 0.125 Å, and the axial locations are occupied $O4^{\#2}$ atom and O1 atom, and the angle of $O4^{\#2}$-Co1-O1 bond is 176.33(7)°. A $N3^{\#4}$ atom and coordinating O7, O6 and O5 atoms come from equatorial plane, and the four equatorial atoms are nearly coplanar with Co2 atom, the average deviation is 0.152 Å. $O10^{\#4}$ atom and $O9^{\#3}$ atom are situated in the two sides of plane, the bond angle of $O9^{\#3}$-Co2-$O10^{\#4}$ is 177.32(6)°. In addition, the Co1 and Co1 atoms (or Co2 and Co2) are successively bridged via carboxylic acid O atom, hydroxyl O atom as well as the imidazole N atom to produce the [$Co_2(HL)_2$] dinuclear unit (Fig. 2b). According to Fig. 2c, *syn, trans* μ_2-1,3-carboxylic acid groups connect the neighboring dimmers to provide an infinite 1-dimensional chain, where the distance of the consecutive Co1···Co2 is 4.8977(5) Å. Finally, via the *syn, trans* carboxyl group exists in H_2L bridge the neighboring chains generating 2-dimensional supramolecular sheet, the square dimensions are 4.9096×10.9069 $Å^2$ (Fig. 2d).

For exploring the products' phase purity, the PXRD study for the as-prepared CPs was finished (Fig. 3a). Between the PXRD patterns peak positions of the simulation and experiment, there exist a well accordance, and this result suggests that the crystal architectures is a real representation of massive crystal products. The strength differences are probably resulted from crystal samples preferred selection. For analyzing the thermal stability of skeletons, the TGA could be involved in a temperature range of 25 °C-800 °C with 10°C per min heating rate under Ar flow (Fig. 3b). Complex **1**

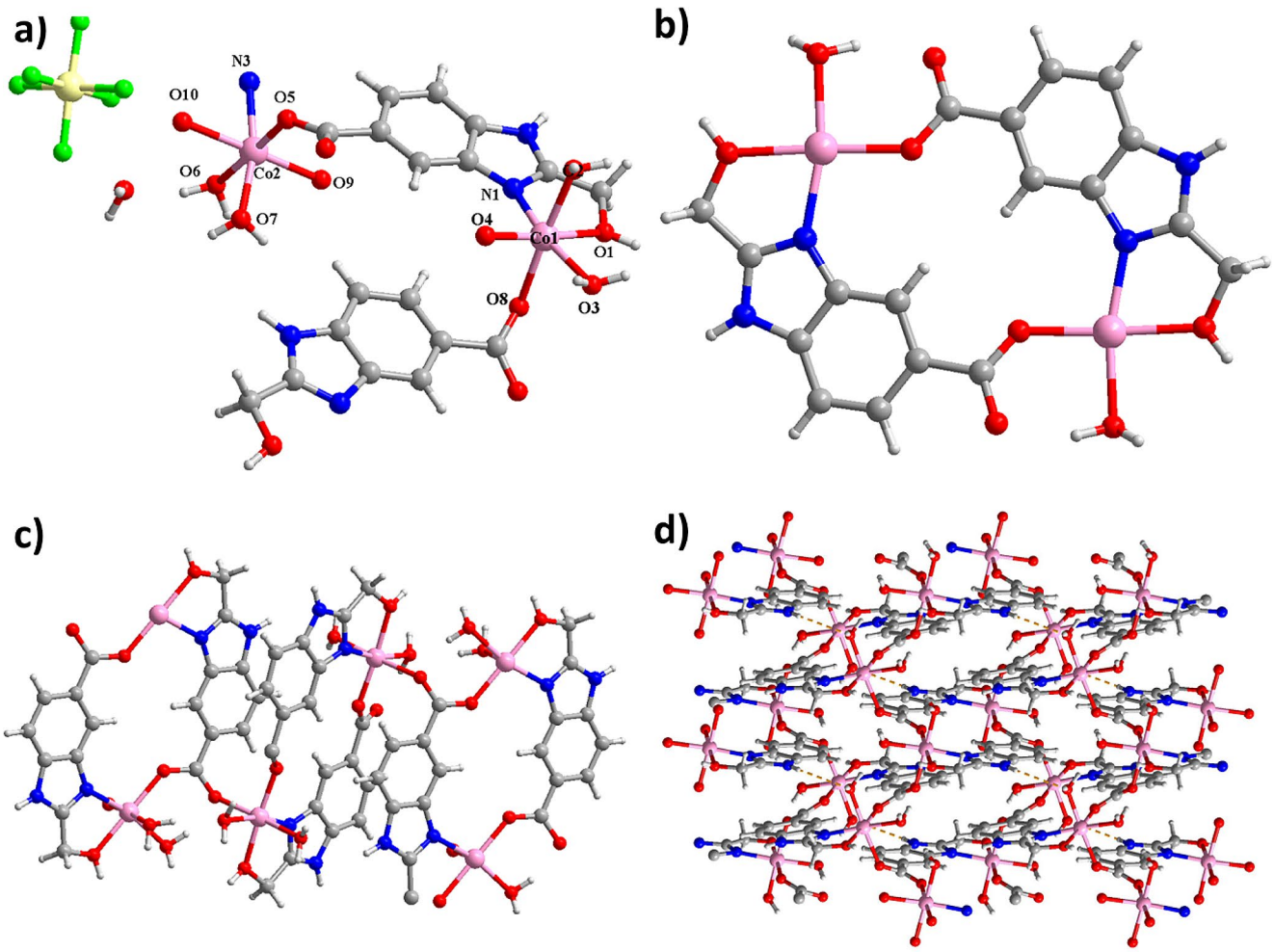

Fig. 2 (a) The diagram of the **2**'s least building unit. (b) [$Co_2(HL)_2$] dinuclear unit of the complex **2**. (c) The 1-dimensional chain architecture exits in compound **2**. (d) **2**'s 2D supramolecular net

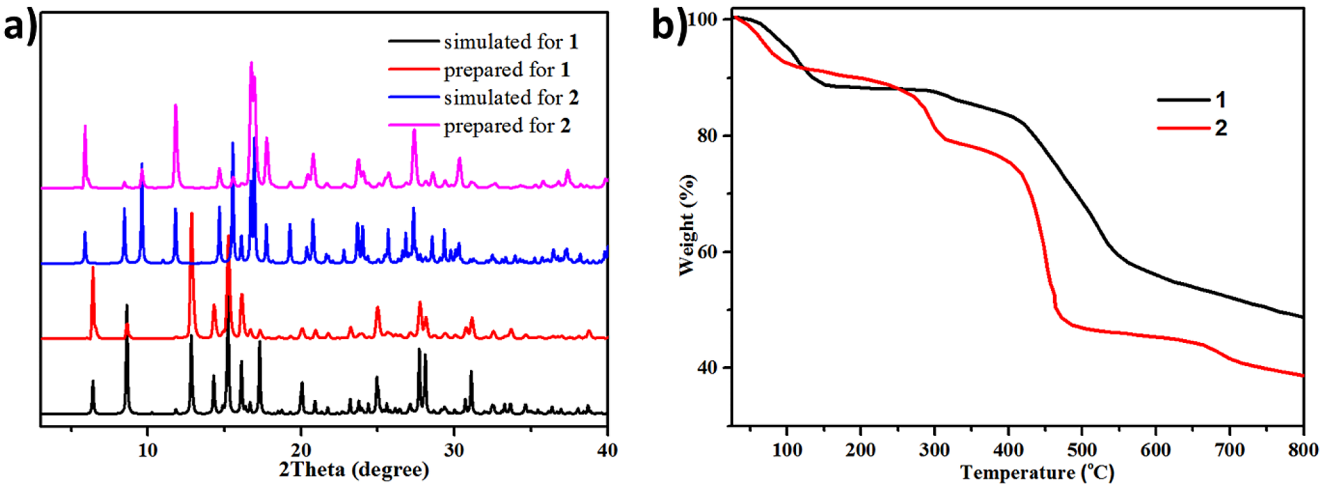

Fig. 3 (a) The CPs' patterns of PXRD. (b) and their curves of TGA.

reflects 10.2% of weightlessness between 60 and 160 °C is on account of the removing a lattice and three coordinated molecules of H_2O (the calculated value is 9.7%). The **2**'s TG curve provides 11.9% of weightlessness between 60 and 147 °C, associated with the losing four coordinated and a lattice molecules of H_2O (the calculated value is 12.2%), and next, in a temperature range of 260–400 °C, 18.8% of the second step weightlessness appears, which is related to the loss of a free SiF_6^{2-} ions (the calculated value is 19.6%).

3.2 Photocatalytic Property

Considering that manganese and cobalt ions are commonly used as efficient active centers for electrocatalytic hydrogen and oxygen evolution or photocatalytic degradation of organic dyes, and the two complexes prepared with the H2L ligand used in this study can absorb both ultraviolet and visible light due to their extended conjugated structures, providing an energy source for dye degradation. Therefore, the two complexes prepared in this study are highly likely to possess photocatalytic degradation performance for dyes. The photocatalytic degradation rates of the two complexes towards the common organic dye RhB were tested using a UV-visible absorption spectrophotometer. As shown in Fig. 4a-b, the initial solution of RhB without complexes exhibited a stable characteristic UV absorption peak at 550 nm. However, upon the addition of 30 mg of finely ground complexes, the characteristic absorption peak of RhB gradually decreased with increasing UV irradiation time and reached its minimum value at 150 min. The UV absorption peak intensities of RhB at different times were collected at 30-minute intervals to describe the degradation process. The collected data were plotted in Fig. 4a-b, which showed that within 150 min, the maximum degradation rates of RhB under the catalysis of complexes **1** and **2** were 88.52% and 80.16%, respectively, indicating the effectiveness of the obtained complexes in RhB degradation. In addition, to evaluate the cycling performance of the obtained samples, a recycling experiment was conducted to study their catalytic efficiency. In the typical recycling experiment, distilled water, 0.1 M NaCl aqueous solution, and ethanol were used as washing agents to restore the catalytic performance of the catalyst. The typical procedure is as follows: collect the complexes after catalytic testing, wash the samples three times sequentially with distilled water, 0.1 M NaCl aqueous solution, and ethanol, then vacuum dry at 80 °C for 6 h. The dried samples were used for subsequent cyclic performance tests. The cyclic performance tests were repeated five times for each group of samples. The obtained data are shown in Fig. 4c-d. The results showed that after five repeated uses, both complexes were able to maintain catalytic efficiency at 82.97% (**1**) and 75.98% (**2**), indicating that the prepared complexes, as photocatalysts for dye degradation, exhibited good cyclic usability.

4 Conclusion

Taken together, we have produced two fresh transition metal CPs in success on the basis of Co(II) and Mn(II) ions as the metal centers with reaction between H_2L and corresponding metal salts under the reaction condition of solvothermal. And their architectures could be characterized via the PXRD, EA, IR, single-crystal X-ray

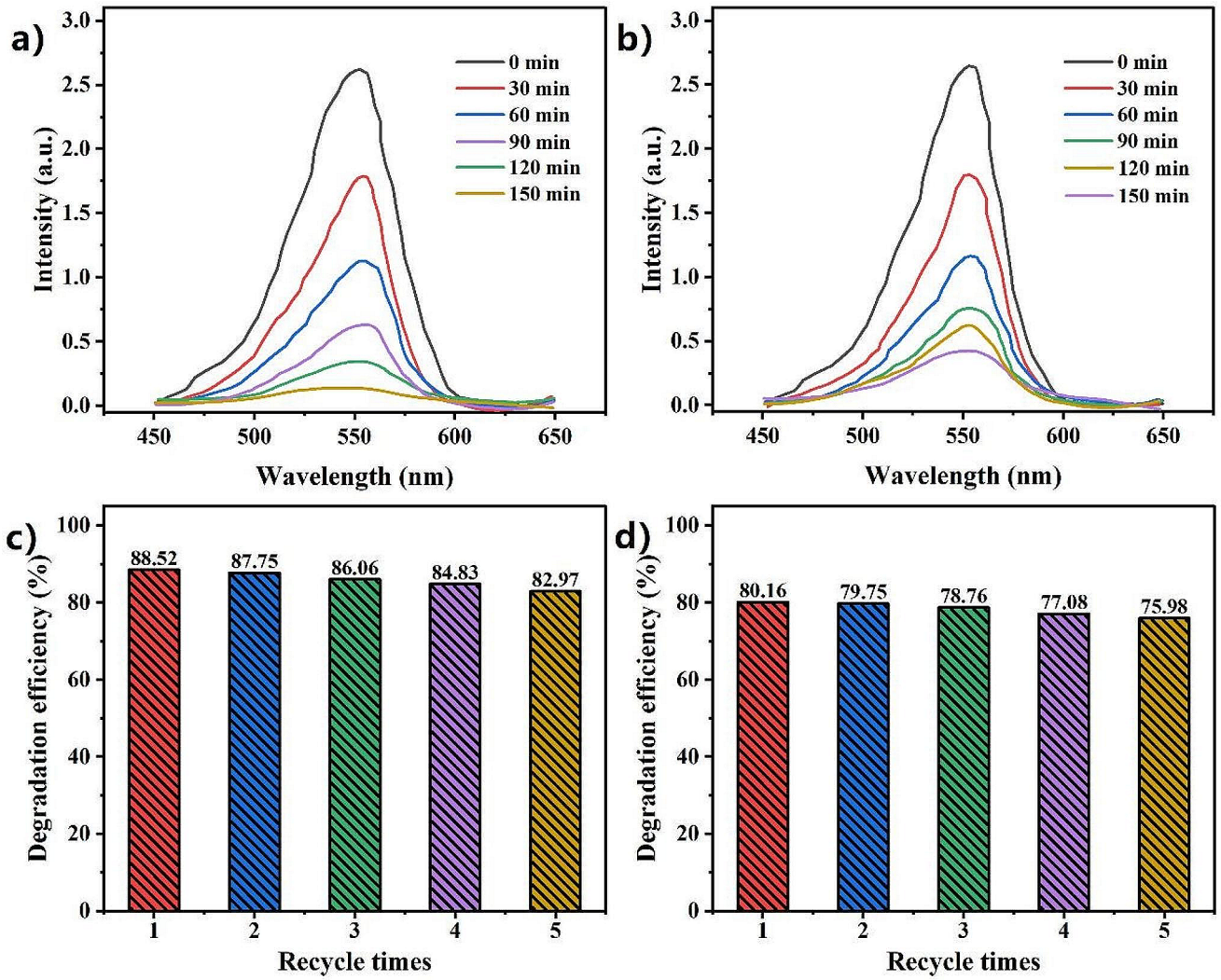

Fig. 4 (a) UV-Vis absorption spectra of RhB with CP **1** under exposure to UV light. (b) UV-Vis absorption spectra of RhB with CP **2** under exposure to UV light. (c) The cyclic performance testing of CP **1**. (d) The cyclic performance testing of CP **2**

diffraction, and TGA. The degradation rate of RhB was investigated using UV-visible spectroscopy. The results indicated that both complexes exhibited excellent photocatalytic degradation efficiency and good recyclability for RhB under UV light irradiation, suggesting their potential application in the treatment of organic dye wastewater.

Author Contributions Jing Li and Liuchang Wang synthesized and characterized the compounds; Hongjiang Ren and Jiangtao Li performed other experiments.

Funding The research was supported by Research on the Application of Inorganic Nanofunctional Composite Materials (XAWLKYTD202312), Natural Science Basic Research Plan in Shaanxi Province of China (2022JM-075) and Three-year action plan project of Xi'an University (21XJZZ0001-11).

Data Availability The data used to support the findings of this study are included within the article.

Declarations

Ethical Approval Not applicable.

Competing Interests The authors declare no competing interests.

References

1. C. Zamora-Ledezma, D. Negrete-Bolagay, F. Figueroa, E. Zamora-Ledezma, M. Ni, F. Alexis, V.H. Guerrero, Heavy metal water pollution: a fresh look about hazards, novel and conventional remediation methods. Environ. Technol. Inno. **22**, 101504 (2021)
2. A. Rafiq, M. Ikram, S. Ali, F. Niaz, M. Khan, Q. Khan, M. Maqbool, Photocatalytic degradation of dyes using semiconductor

photocatalysts to clean industrial water pollution. J. Ind. Eng. Chem. **97**, 111–128 (2021)
3. Y. Zhang, J. Wang, J. Lu, J. Wu, Antibiotic resistance genes might serve as new indicators for wastewater contamination of coastal waters: spatial distribution and source apportionment of antibiotic resistance genes in a coastal bay. Ecol. Indic. **114**, 106299 (2020)
4. N. Lei, H. Wang, L. Fan, X. Chen, Highly luminescent soft aggregates and films assembled by amphiphilic polyoxometalate complex in a polymerizable aprotic ionic liquid. J. Photoch Photobio A **448**, 115290 (2024)
5. T. Sabithakala, V.R.R. Chittireddy, DNA binding and in vitro anticancer activity of 2-((1 H -benzimidazol-2-yl)methylamino) acetic acid and its copper(II) mixed-polypyridyl complexes: synthesis and crystal structure. Appl. Organomet. Chem. **32**, e4550 (2018)
6. N. Lei, W. Li, D. Zhao, W. Li, X. Liu, L. Liu, J. Yin, M. Muddassir, R. Wen, L. Fan, A bifunctional luminescence sensor for biomarkers detection in serum and urine based on Chemorobust Nickel(II) metal-organic Framework. Spectrochim. Acta A **306**, 123585 (2024)
7. L. Fan, D. Zhao, B. Li, F. Wang, Y. Deng, Y. Peng, X. Wang, X. Zhang, Luminescent binuclear zinc(II) organic framework as bifunctional water-stable chemosensor for efficient detection of antibiotics and cr(VI) anions in water. Spectrochim. Acta Part A Mol. Biomol. Spectrosc. **264**, 120232 (2022)
8. W. Li, W. Li, X. Liu, D. Zhao, L. Liu, J. Yin, X. Li, G. Zhang, L. Fan, Two Chemorobust Cobalt(II) Organic frameworks as high sensitivity and selectivity sensors for efficient detection of 3-Nitrotyrosine biomarker in serum. Cryst. Growth Des. **23**, 7716–7724 (2023)
9. Y.Q. Feng, Z.G. Zhong, S.Y. Chen, K.C. Liu, Z.H. Meng, Improved Catalytic Performance toward Selective Oxidation of Benzyl Alcohols originated from New Open-Framework copper molybdovanadate with a Unique V/Mo Ratio. Chem. Eur. J. **29**, e202302051 (2023)
10. J. Zhao, Z. Dang, M. Muddassir, S. Raza, A. Zhong, X. Wang, J. Jin, A new cd(II)-Based coordination polymer for efficient photocatalytic removal of Organic dyes. Molecules. **28**, 3848 (2023)
11. L. Qin, F. Liang, Y. Li, J. Wu, S. Guan, M. Wu, S. Xie, M. Luo, D. Ma, A 2D Porous Zinc-Organic Framework platform for loading of 5-Fluorouracil. Inorganics. **10**, 202 (2022)
12. X. Dong, Y. Li, D. Li, D. Liao, T. Qin, O. Prakash, A. Kumar, J. Liu, A new 3D 8-connected cd(ii) MOF as a potent photocatalyst for oxytetracycline antibiotic degradation. CrystEngComm. **24**, 6933–6943 (2022)
13. Y.M. Zhao, G.M. Tang, Y.T. Wang, Y.Z. Cui, S.W. Ng, Copper-based metal coordination complexes with voriconazole ligand: syntheses, structures and antimicrobial properties. J. Solid State Chem. **259**, 19–27 (2018)
14. T.A. Fernandes, I.F.M. Costa, P. Jorge, A.C. Sousa, V. André, N. Cerca, A.M. Kirillov, Silver(I) coordination polymers immobilized into Biopolymer films for Antimicrobial Applications. ACS Appl. Mater. Interfaces. **13**, 12836–12844 (2021)
15. D.S. Raja, N.S.P. Bhuvanesh, K. Natarajan, A novel water soluble ligand bridged cobalt(ii) coordination polymer of 2-oxo-1,2-dihydroquinoline-3-carbaldehyde (isonicotinic) hydrazone: evaluation of the DNA binding, protein interaction, radical scavenging and anticancer activity. Dalt Trans. **41**, 4365 (2012)
16. T. Karmakar, Y. Kuang, N. Neamati, J.B. Baruah, Cadmium complexes and cocrystals of indium complexes of benzothiazole derivatives and anticancer activities of the cadmium complexes. Polyhedron. **54**, 285–293 (2013)
17. N. Alvarez, L.F.S. Mendes, M.G. Kramer, M.H. Torre, A.J. Costa-Filho, J. Ellena, G. Facchin, Development of copper(II)-diimine-iminodiacetate mixed ligand complexes as potential antitumor agents. Inorganica Chim. Acta. **483**, 61–70 (2018)
18. J. Shen, W. He, The fabrication strategies of near-infrared absorbing transition metal complexes. Coordin Chem. Rev. **483**, 215096 (2023)
19. M.B. Thoke, G.J. Sun, R.A. Borse, P. Lin, S.X. Lin, Unimolecular cooperative metallaphotocatalysis with conjugately bridged Ir–Ni complexes and its applications in organic coupling reactions. Org. Chem. Front. **9**, 1797–1807 (2022)
20. M.Y. Rather, M. Shincy, S.M. Sundarapandian, Photocatalytic degradation of Rhodamine-B by phytosynthesized gold nanoparticles. Int. J. Environ. Sci. Te. **20**, 4073–4084 (2023)
21. M. Chin, C. Cisneros, Stephanie m., K.M. Araiza, K.M. Vargas, F. Ishihara, Tian, Rhodamine B degradation by nanosized zeolitic imidazolate framework-8 (ZIF-8). RSC Adv. 8, 26987–26997 (2018)
22. K. Vijayan, S.P. Vijayachamundeeswari, Improving the multifunctional attributes and photocatalytic dye degradation of MB and RhB dye – A comparative scrutiny. Inorg. Chem. Commun. **144**, 109940 (2022)